Effects of Loading Characteristics on the Performance of Sliding Isolation Devices

G. Lomiento, N. Bonessio & G. Benzoni
University of California, San Diego
Department of Structural Engineering
La Jolla, CA 92093-0085, U.S.A.
glomiento@ucsd.edu, nbonessio@ucsd.edu, gbenzoni@ucsd.edu

15 WCEE
LISBOA 2012

SUMMARY:
Devices with large displacement capability and stable energy dissipation are desirable for the protection against earthquake loads. The use of sliding bearings in buildings and bridges is extensively increasing for the above mentioned performance as well as for their compact shape and the advantages introduced by new materials. In this paper the results of dynamic tests on concave sliding isolators are presented. The response of devices was studied in a wide velocity range, for mono-directional and bi-directional motions with variation of the applied vertical load. The experimental phase of the study indicated performance characteristics that should be taken into consideration for the design of structures equipped with this technology. For this goal, a numerical model, able to account for the observed device performance characteristics, is proposed.

Keywords: seismic isolation, sliding concave bearings, full scale tests.

1. INTRODUCTION

Concave sliding bearings are suitable for a wide range of applications for buildings, bridges and industrial facilities, due to their relevant features: a quite compact shape, with considerably lower height with respect to elastomeric bearings of similar capabilities, large displacement capacity, and natural frequency imposed on the structure dependent only on the sliding surface radius and not on the supported mass.

A considerable literature on experimental and analytical analyses of these devices is available (Zayas et al., 1987; Zayas et al., 1989; Zayas et al., 1990; Mokha et al. 1991; Mokha et al., 1993; Bondonee and Filiatrault, 2002). Experimental data confirm that the coefficient of friction depends on (1) the vertical applied load, (2) the sliding velocity and (3) the direction of motion. These effects are well documented and included in consolidated models (Tsai, 1997; Mosqueda et al., 2004) and proved to affect the behaviour of sliding devices during the earthquake shaking in terms of forces and displacements across the isolator. Tests on full scale devices, completed in more recent years, documented the degradation of the frictional characteristics due to the generation of high temperatures at the sliding interface during reversal cycles of motion. However, test protocols were often project specific, resulting in a database of results of difficult interpretation for the design of a realistic model of the device performance. For this reason, a systematic investigation of the bearing performance across a range of realistic vertical loads and velocities inspired this research effort.
In this paper a model able to include the effects of (1) the applied load, (2) the sliding velocity, and (3) the degradation of the friction coefficient during repetitive cycles is presented. The focus of the paper is on short duration motion and low wear, typical of earthquake excitation.

Even though the results obtained cannot be considered representative of all the possible scenarios experienced by the isolators in their service life, they indicate that models neglecting the above mentioned effects can lead to unsatisfactory assessments of the structural response during an earthquake.

2. EXPERIMENTAL CAMPAIGN

A set of sliding bearings, with concave surface, was tested under three values of vertical load for a two-cycles sinusoidal input with fixed displacement range and ten different peak velocities. The effective radius of the concave surface of these specific bearings is 2650 mm, and the low friction material that interfaces the stainless steel concave surface is an un-lubricated polymer composite liner with about 400 MPa compressive yield strength.

2.1. Testing protocol

The devices were tested at the Caltrans SRMD Testing Facility at the University of California San Diego campus equipped with a 6 DOFs shake table specifically designed for full scale testing of isolators and energy dissipators (Benzoni and Seible, 1998). The displacement range of the table in longitudinal direction is +/- 1.22 m with a maximum horizontal capacity of 9000 kN and a vertical load capacity of 53400 kN. The peak velocity of the table longitudinal motion is 1.8 m/s. The installation procedure of the devices on the testing machine is consistent with the standard installation of isolation devices. The device base is typically connected to the table and the top portion, above the slider, is bolted to the vertical reaction frame that represents a fixed reference. The table is raised imposing the desired vertical load to the device and then commanded to the requested 3D motion. A schematic of the tested devices is shown in **Fig. 1**.

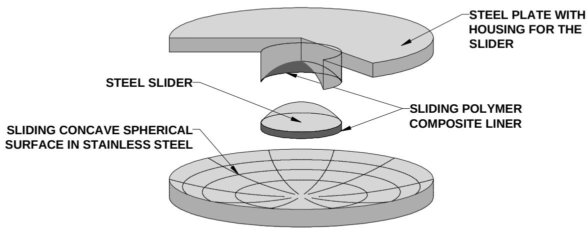

Figure 1. Schematic of concave sliding bearing

The tests are divided in three categories based on the applied vertical load *W*. Specifically, the vertical loads of 3263 KN, 6525 KN and 13050 KN, corresponding respectively to a pressure *p* of 15, 30 and 60 MPa, were applied. The medium load (*W*=6525 KN) represents the design vertical load for the devices. For each set of loads, mono-directional tests were completed at 10 peak sliding velocity levels ranging from 0.254 mm/s to 800 mm/s (0.254, 1.27, 5, 10, 20, 50, 100, 200 400, 800 mm/s). Two fully reversed sinusoidal cycles, with displacement amplitude *D*=200 mm were applied for all the mono-directional tests. Bi-directional cloverleaf tests were also completed with maximum displacement of 200 mm in longitudinal direction and 100 mm in lateral direction. The peak velocities of 90 mm/s and 45 mm/s were applied in longitudinal and lateral direction, respectively.

The displacement pattern in the horizontal plane of cloverleaf tests is shown in Fig. 2(a). The applied displacement time histories in the two perpendicular directions are reported in Fig. 2(b). It must be noted that loops of limited amplitude are applied at the beginning and end of each run in order to avoid excessive levels of acceleration. For better interpretation of the bi-directional test results, two tests were performed, under pressure of 30 Mpa, separately in longitudinal and lateral direction up to the displacement levels that were used as components of the cloverleaf tests.

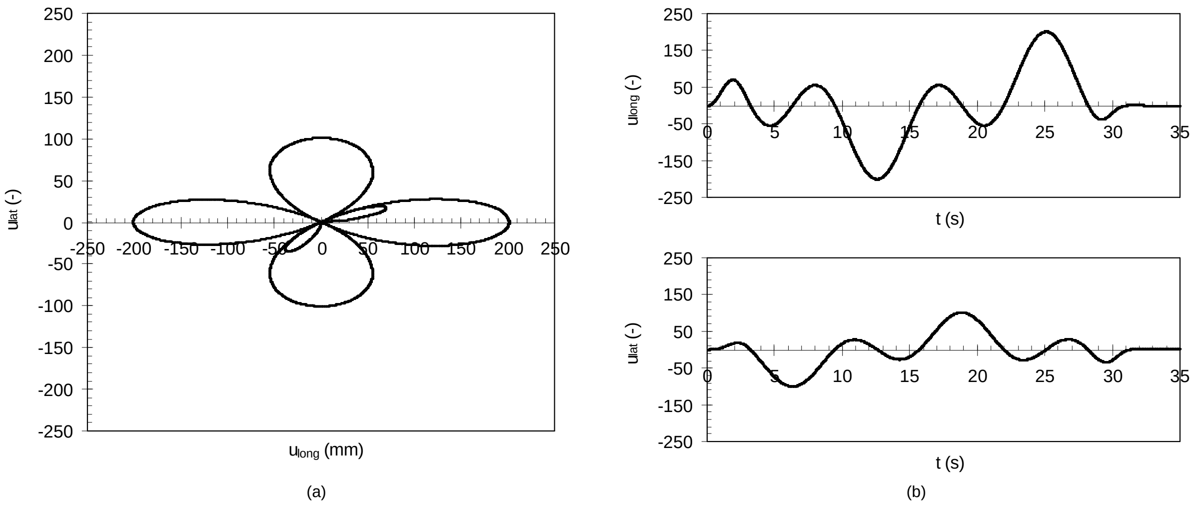

Figure 2. Cloverleaf test displacements: (a) trajectory and (b) longitudinal and lateral components of motion.

2.2. Experimental evidence

According to the simplified analytical model of the bilinear behavior of sliding concave isolators, developed by Zayas et al. (1989, 1990), the force-displacement relationship for a generic direction of sliding is expressed as:

$$F = \frac{W}{R} u + sign(v)\mu W \tag{2.1}$$

where W represents the applied vertical load, u the horizontal relative displacement between slider and concave base, v the velocity, R the radius of the concave surface, μ the friction coefficient of the sliding system (composite material at the bottom of the slider and stainless steel overlay of the concave base) and F the horizontal restoring force. The horizontal force is partially resisted by the force generated by the frictional characteristics of the contact surfaces μW. The remaining force is resisted by the component associated with the "restoring stiffness":

$$K_{ra} = \frac{W}{R}\,. \tag{2.2}$$

For each mono-directional test performed, the restoring stiffness K_{ra} was evaluated as the average between the slope of the upper and lower portion of the force-displacement loops, obtained with best fit interpolation of the experimental data. The variation of K_{ra} with applied loads and peak test velocities is presented in Fig. 3(a) and Fig. 3(b), respectively. The theoretical values of stiffness of Eq. 2.2 are indicated with a dotted line. The least-squares fit of the experimental data appears to closely match the theoretical prediction, for different pressure levels. For different vertical loads and peak velocity V an initial increase of stiffness with velocity up to about 10 mm/s was noticed. The lower vertical load case (p=15 Mpa) appears to experience a reduction of restoring stiffness for velocity around 200 mm/s, followed by an increasing trend for very high velocities. This phase of reduction is generally not experienced for higher vertical load cases that indicate instead a more pronounced increment of stiffness with velocity. A significant reduction of restoring stiffness from first to second cycle is visible only for the higher pressure (p=60 Mpa). The disagreement between experimental and theoretically values of K_{ra} is in general limited, not exceeding 16%, 5% and 7%, for the three increasing vertical loads, respectively.

Even though the theoretical definition of Eq. 2.2 neglects secondary effects related, for instance, to the development of frictional forces at the rotating interface between slider and the top housing of the device, the agreement between experimental and theoretical results appears sufficient to justify the use of Eq. 2.2 as representative of the restoring behaviour.

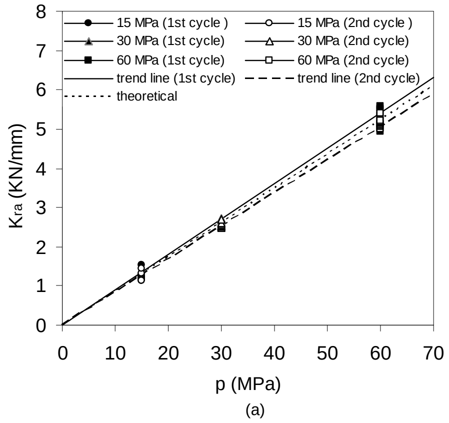

Figure 3. Restoring stiffness at different pressures (a) and testing peak velocities (b).

2.2.2. Coefficient of friction

In order to underline the pure frictional performance, the force component associated with the restoring stiffness was removed from the experimental data. The remaining force, divided by the applied vertical load, provides the experimental friction coefficient. This parameter (μ) is reported in Fig. 4 versus the device displacement u for a sample of data results from mono-directional tests at 100 mm/s. The plot of Fig. 4(a) is for an applied pressure of 15 MPa, while in Fig. 4(b) results for a pressure of 30 MPa are presented.

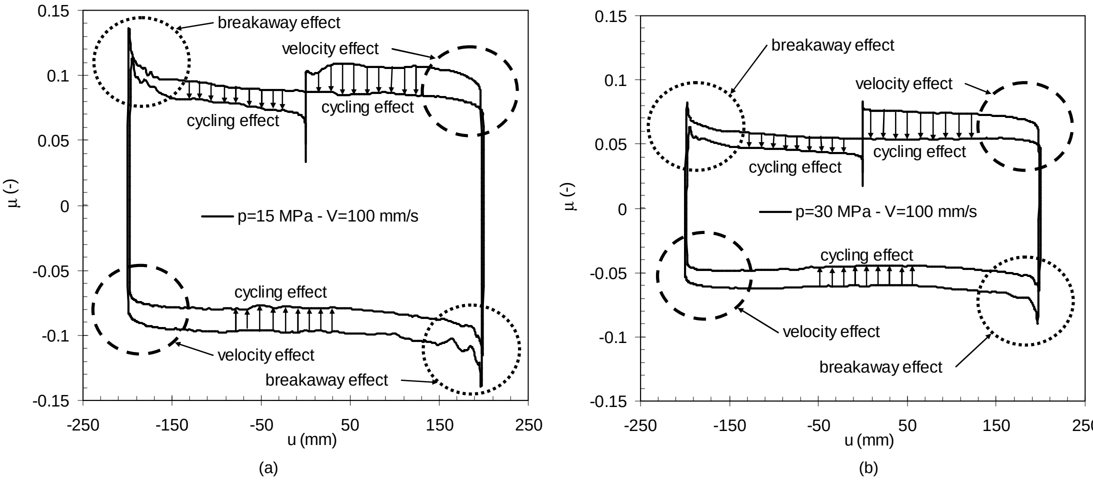

Figure 4. Frictional coefficient-displacement loop from tests with V=100 mm/s for: a) p=15 MPa (W=3263 kN), b) p=30 MPa (W=6525 kN).

According to the simplified Coulomb model, the frictional force is directly proportional to the applied load, independent on the apparent area of contact and sliding velocity. This assumption would result in a rectangular friction coefficient-displacement loop in clear disagreement with the experimentally obtained shapes. The analysis of the shape of the loops indicates four major effects, related to the frictional performance of the device, responsible for the departure from the theoretical Coulomb's model:

1. a "breakaway effect" appearing as a sudden increase of coefficient of friction at the beginning of the motion or at each motion reversal. This effect relates both to the static friction condition as well as to stick-slip, intended as short duration increase of the frictional force followed by a rapid release of force. Both phenomena involve (i) a momentary sticking of the interfaces and (ii) acceleration impulses. The breakaway effect is clearly visible in all the tests, as shown in

the dotted circles of Fig. 4(a) and (b).

2. A "load effect", as a reduction of the friction coefficient for increasing vertical load. Comparing, for instance, the results of Fig. 4(a) and Fig. 4(b) it can be noted that the friction coefficient varies with increasing vertical load from approximately 0.08 to 0.05.
3. A "cycling effect", that shows as a continue reduction of the friction coefficient with the repetition of cycles, more pronounced for higher velocity tests. The plots of Fig. 4(a) and Fig. 4(b) show a 2nd loop narrower than the 1st loop, indicating a decrement of the coefficient of friction with the travelled path.
4. A "velocity effect", responsible for the variation of the friction coefficient with velocity of motion. A reduction of speed is expected to introduce lower values of friction coefficient. This reduction can be observed in the rounding of the shape of the loops when approaching the peak displacement in the dashed areas of Fig. 4(a) and 4(b). In these areas, due to the sinusoidal type of excitation, the velocity is decreasing with a consequent drop of the friction coefficient value.

These effects were observed for every test completed for this project. For simplicity they were analyzed in detail for mono-directional test only, as presented in what follows. However, the bi-directional tests indicated additional effects, visualized in Fig. 5 were both the overall bi-directional response as well as the associated orthogonal response components are reported.

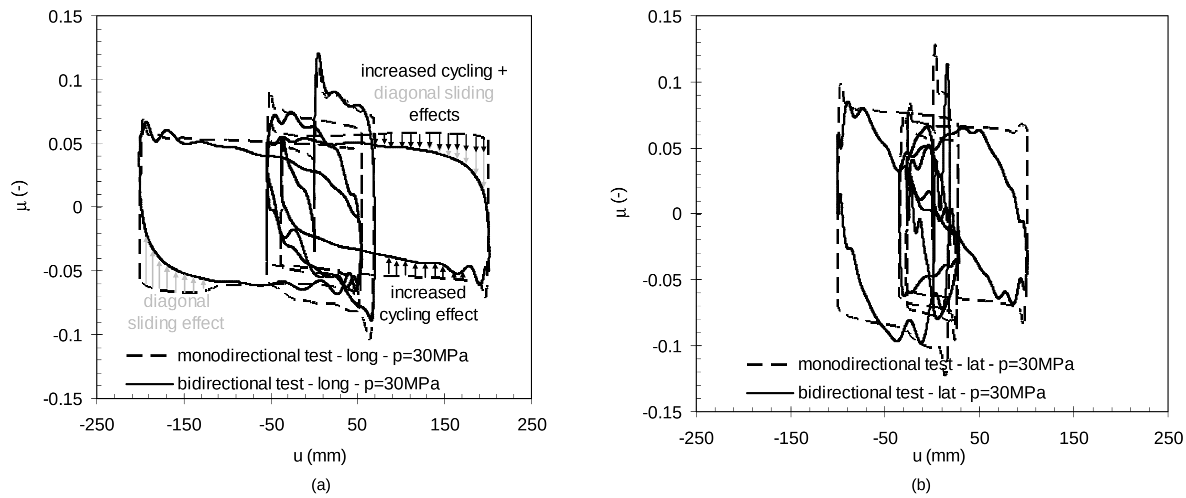

Figure 5. Bi-directional and mono-directional experimental loops for p=30 MPa (W=6525 kN): (a) longitudinal and (b) lateral direction.

5. A "diagonal sliding effect". During the applied bi-directional motion the slider moves along directions not parallel to the longitudinal and lateral axis of the device. The frictional force developed in longitudinal and lateral direction is only a component of the force generated along the diagonal direction. For this reason, the bi-directional experimental cycles indicate an apparent reduction of the frictional force with respect to the mono-directional results. This effect is particularly visible in Fig. 5 in the higher displacement regions. It must be noted that the reduction of μ in Fig. 5(a) from mono-directional to bi-directional response is also contributed by an additional increase of temperature during the bi-directional motion (increased cycling).
6. An "asymmetry effect". Due to the manufacturing process of the sliding surfaces, the friction coefficient depends on the direction of motion. In Fig. 5, for instance, the loops in the lateral direction show larger values of μ than in the longitudinal direction due to both velocity and asymmetric effects.

In Fig. 6 the coefficient of friction components in longitudinal and lateral direction are reported for cloverleaf tests at different level of applied pressure. The slightly elliptical shape documents the above mentioned velocity and asymmetry effects while the disturbances in the loops (theoretically circular) are attributed to the breakaway and velocity effects. The radius of the loop reduces with increasing pressure and repetition of cycles (cycling effect) that justify the spiral shape.

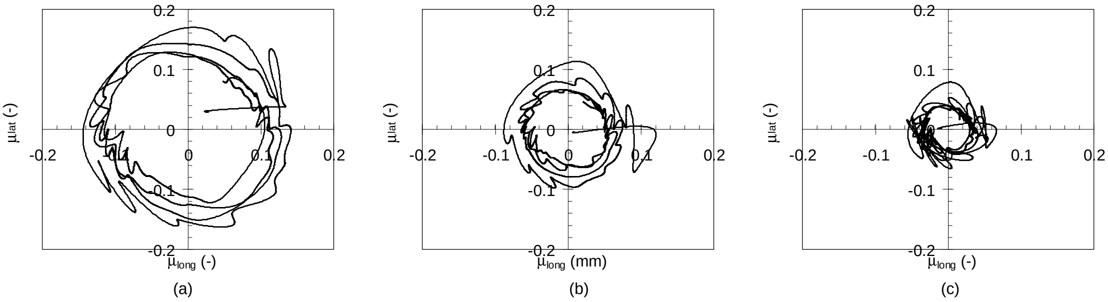

Figure 6. Longitudinal-lateral friction interaction diagram: (a) *p*=15 MPa, (b) *p*=30 MPa and (c) *p*=60 MPa.

While the transition between static and dynamic phase of sliding has been found to be dependent on the vertical load and velocity but appears to have limited impact on the amount of dissipated energy (Mokha et al. 1993, Bondonee et al. 2002, Soong et al. 2004), effect 2 to 5 (i.e. load, cycling, velocity, asymmetry, and diagonal sliding) directly affect the dissipation capacity of the devices and, in the author's opinion, should be included in a correct model of the device performance to prevent possible underestimates of the peak displacement of the isolated structure during a seismic event. Effect 6) is currently under further study at the University of California San Diego.

2. PROPOSED MODEL

Numerical models of the performance of a sliding isolation system have been reported in (Constantinou et al., 1990; Mokha et al., 1993; Deb and Paul, 2000, Tsopelas et al., 1996, Mosqueda et al., 2004), mainly with the scope of evaluating the effects of bearing pressure, sliding velocity, breakaway friction and bi-directional motion on the seismic response of base-isolated structures. A phenomenological model able to take into account the load and velocity effects together with the variation of the friction characteristics along the travelled path (cycling effect) has been recently proposed by Lomiento et al. (2012). This model has been calibrated on mono-directional tests and is expressed as the product of three components:

$$\mu(W, c, v) = f_W(W) \cdot f_c(c) \cdot f_v(v). \tag{3.1}$$

The "load effect" is represented by the function

$$f_W(W) = \mu_{s0} e^{-W/W_{ref}} \tag{3.2}$$

where $\mu_{s,0}$ and W_{ref} are reference coefficient of friction and applied load, while W is the applied vertical load. The values $\mu_{s,0}$ = 0.103 and W_{ref} = 12300 kN were determined with a least squares regression over the experimental data from slow motion tests with peak velocity $V \leq 5$mm/s.

The function that represents the "cycling effect" is introduced as:

$$f_c(c) = e^{-(c/c_{ref})^{\beta}} \tag{3.3}$$

where the parameter c relates to the heat flux developed at the contact surface, and c_{ref} is a reference value obtained by least square regression of the experimental results. The term c is defined as:

$$c(t) = \frac{2}{a\pi^2 A^2} \int_{t_0}^{t} W v^2 dt \tag{3.4}$$

were a is the radius of the slider, A is the radius of curvature of the concave surface, and β represents the frictional degradation rate. For the performed tests, the values c_{ref} = 6600 kN/ms and β = 0.5 were obtained.

The load effect is introduced by the function:

$$f_v(v) = \gamma + (1-\gamma)e^{-|v|/v_{ref}} \tag{3.5}$$

where v is the sliding velocity, v_{ref} is a reference velocity, and $\gamma \geq 1$ express the ratio between the fast-motion and the slow-motion coefficient of friction. The values γ = 1.4 and v_{ref} = 10 mm/s have been found as best fit of the experimental data.

In multi-directional movements, the velocity and the displacement across the isolator can be expressed by the vectors $\mathbf{u} = \begin{bmatrix} u_x & u_y \end{bmatrix}^{\mathrm{T}}$ and $\mathbf{v} = \begin{bmatrix} v_x & v_y \end{bmatrix}^{\mathrm{T}}$, respectively. The proposed force-displacement relationship, taking into account the "diagonal sliding effect" is:

$$\begin{bmatrix} F_x \\ F_y \end{bmatrix} = \frac{W}{R}\begin{bmatrix} u_x \\ u_y \end{bmatrix} + \mu(W,c,v)W\frac{1}{|\mathbf{v}|}\begin{bmatrix} v_x \\ v_y \end{bmatrix} \tag{3.6}$$

It must be noted that effects 2, 3, and 4 are included in Eq. 3.6 through the parameter $\mu(W,c,v)$ obtained by Eq. 3.1, while the bi-directional type of loading is considered by the vector $\frac{1}{|\mathbf{v}|}\begin{bmatrix} v_x \\ v_y \end{bmatrix}$. The use of perpendicular components of velocity (v_x and v_y) assumes that the frictional force acts in the same direction of the sliding velocity (Mosqueda et al. 2004). While this assumption is valid for flat sliding surfaces it seems to be contradicted by experimental evidence of the device performance. In Fig. 7 the angle of the frictional force (solid line) and velocity (dashed line) are compared for three bi-directional tests under different pressure level.

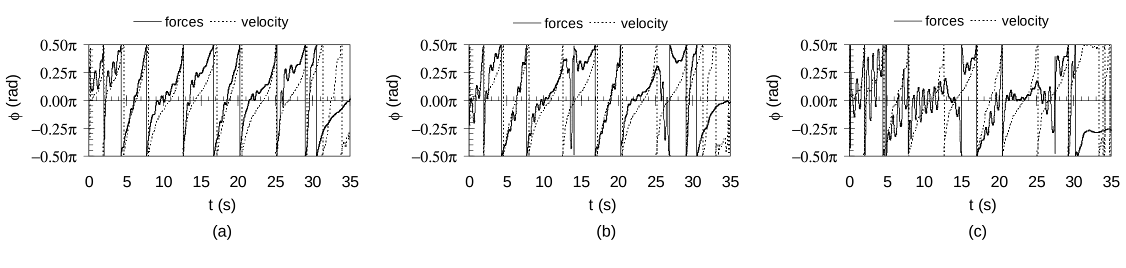

Figure 7. Angle ϕ of frictional force and sliding velocity: (a) p=15 MPa, (b) p=30 MPa and (c) p=60 MPa.

The trend of the force angle is similar but not identical to the velocity angle. This disagreement, increasing with pressure, suggests the existence of a frictional force component opposing the sliding movement and perpendicular to the motion direction. This occurrence, due to the concave shape of the surface, is still under investigation by the authors. For this reason, the above mentioned assumption was retained in this preliminary formulation of the model.

3. EXPERIMENTAL MODEL VALIDATION

The effects accounted for in Eq. 3.1 are visualized in Fig. 8(a) that shows the variation of friction coefficient as function of velocity v and parameter c (Eq. 3.4). The plot refers to the cloverleaf test at p=30 Mpa. During the motion, the coefficient of friction describes the solid line on the surface from point A to B, increasing with velocity and decreasing with increments of c. It must be noted that the parameter c is constantly increasing during the test due to the temperature rise on the sliding surface.

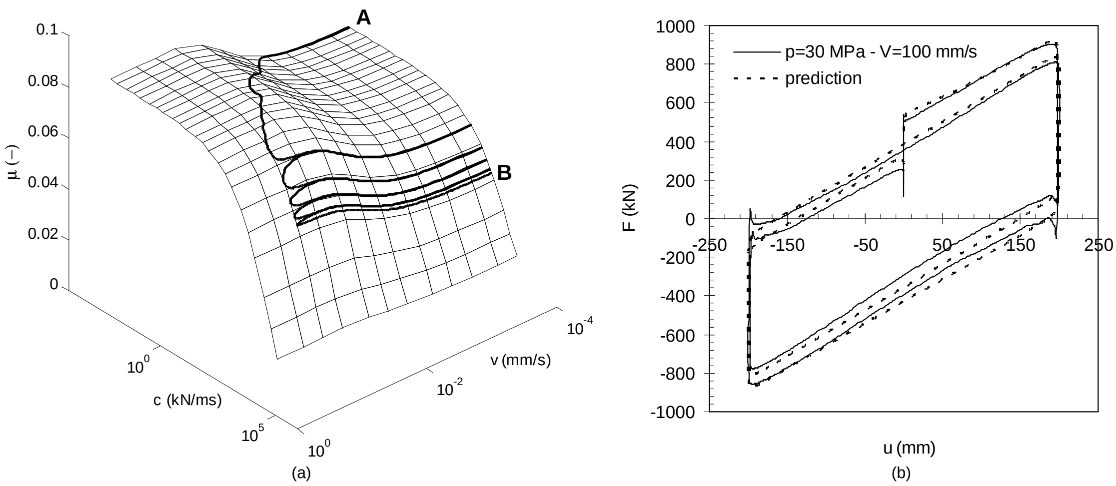

Figure 8. Test at p=30 MPa (W=6525 kN), V=100 mm/s: (a) friction coefficient "trajectory" over the surface of the proposed model, (b) experimental and predicted frictional coefficient-displacement loop.

The proposed model response was compared with the experimental data in terms of force-displacement loops. The behavior is presented in Fig. 8(b) and Fig. 9 for mono-directional and bi-directional tests, respectively. For these plots the force component due to the restoring stiffness was included (slope of the loop).

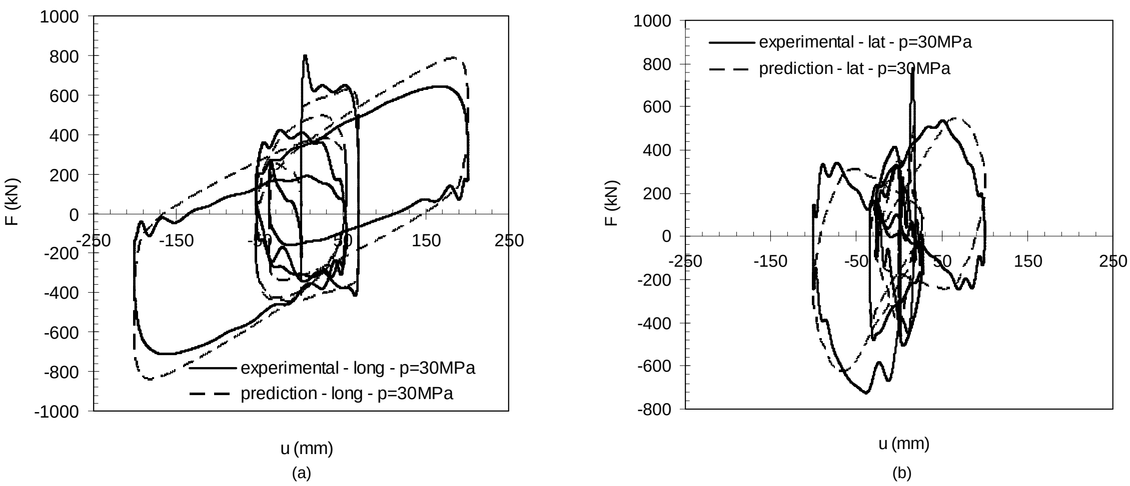

Figure 9. Bi-directional and mono-directional experimental loops for p=30 MPa (W=6525 kN): (a) longitudinal and (b) lateral direction.

The agreement between experimental and numerical response appears satisfactory for mono-directional tests. For bi-directional response the model seems to suffer of the simplification about the relationship between angle of the frictional force and of the velocity vector. The degradation of the friction coefficient during bi-directional tests is, in fact, satisfactorily modeled, as shown in Fig. 10. The two components (longitudinal and lateral) of the coefficient of friction (dotted line) predicted by

Eq. 3.1 are in close agreement in terms of amplitude with the experimental data during the all duration of the tests, but slightly shifted because of errors in the predicted direction.

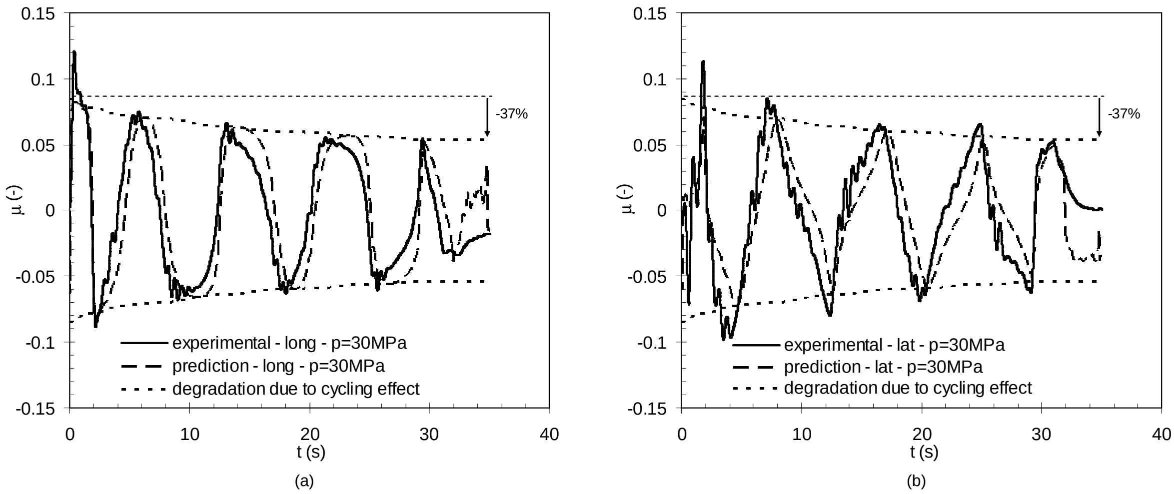

Figure 10. Bi-directional and mono-directional frictional coefficient vs time for the cloverleaf test at *p*=30 MPa: (a) longitudinal component, (b) lateral component.

In order to quantify the accuracy of the model in terms of energy dissipated, in Fig. 11(a), 11(b) and 11(c) the experimental dissipated energy values are presented, for tests with *p*=15, 30 and 60 MPa, respectively. Experimental values are compared with values predicted by the proposed model (L+V+C=Load+Velocity+Cycling) and two partial models including load and velocity effects (L+V) and load effect (L) only.

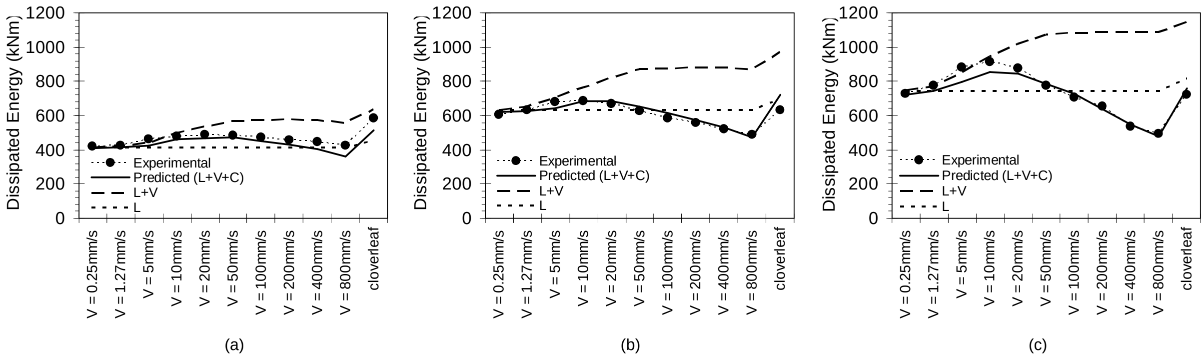

Figure 11. Experimental and predicted dissipated energy: (a) *p*=15 MPa, (b) *p*=30 MPa and (c) *p*=60 MPa.

The model (L) that takes into account only the vertical load effect appears of acceptable accuracy for low velocity conditions only (V≤1.27 mm/s). The model (L+V) including both vertical load and velocity effects, while neglecting the variation of the friction coefficient due to cycling, over-estimates the dissipated energy with an error increasing with velocity and applied load. The complete model (L+V+C) closely matches the test results with a maximum error of 15% of the experimental values.

4. CONCLUSIONS

This paper presents a model of the performance of concave sliding isolation devices based on three independent functions that take into account the effects of applied load, sliding velocity, cycling degradation and diagonal sliding on the friction coefficient. The model is applicable for short duration motion and low wear condition of the sliding material. The proposed model allowed the assessment of the contribution of each effect to the device energy dissipation capability. Results indicated that neglecting the effect of cycle repetitions, and the consequent temperature rise on the sliding surface, can lead to a severe over-estimate of the capacity of the device to dissipate energy. Neglecting the documented variations of the frictional characteristics of these devices can result in an incorrect assessment of displacements levels of the isolated structure during a seismic event.

REFERENCES

Benzoni, G. and Seible, F. (1998). Design of The Caltrans Seismic Response Modification Device (SRMD) Test Facility". *USA – ITALY Workshop on Protective Systems*. Report No. MCEER-98-0015, Multidisciplinary Center for Earthquake Engineering Research, Buffalo, New York City.

Bondonet, G. and Filiatrault, A. (1997). Frictional Response of PTFE Sliding bearings at Higher Frequencies. *Journal of Bridge Engineering.* **2:4**, 139-148.

Constantinou, M. C., Mokha, A. and Reinhorn, A. (1990). Teflon Bearings in Base Isolation, Part II: Modeling. *Journal of Structural Engineering.* **116:2** 455-474.

Constantinou, M. C., Tsopelas, P., Kasalanati, A. and Wolff, E. (1999). Property Modification Factors for Seismic Isolation Bearings. Technical Report MCEER-99-0012, Multidisciplinary Center for Earthquake Engineering Research, Buffalo, NY.

Deb, S. K. and Paul, D. K. (2000). Seismic response of buildings isolated by sliding-elastomer bearings subjected to bi-directional motion. *12th World Conference on Earthquake Engineering*, Auckland, New Zealand.

Dolce, M., Cardone, D. and Croatto, F. (2005). Frictional Behavior of Steel-PTFE Interfaces for Seismic Isolation. *Bulletin of Earthquake Engineering.* **3:1**,75–99.

Lomiento, G., Bonessio, N., and Benzoni, G. (2012). Friction model for sliding bearings under short duration motion. Submitted to *Journal of Earthquake Engineering*.

Mokha, A., Constantinou, M. C., Reinhorn, A. M. and Zayas, V. (1991). Experimental study of friction pendulum isolation system. *Journal of Structural Engineering.* **117:4**, 1201-1217.

Mokha, A., Constantinou, M. C., and Reinhorn, A. M. □(1993). Verification of friction model of teflon bearings under triaxial load. *Journal of Structural Engineering.* **119:1**, 240–261.

Mosqueda, G., Whittaker, A.S., and Fenves, G.L. (2004). Characterization and Modeling of Friction Pendulum Bearings Subjected to Multiple Components of Excitation. *Journal of Structural Engineering.* **130:3**, 423-432.

Soong, T. T., Constantinou, M. C. (1994). Passive and active structural vibration control in civil engineering, Springer, New York.

Tsopelas, P., Constantinou, M. C., Okamoto, S., Fuji, S. and Ozaki, D. (1996). Experimental study of bridge seismic sliding isolation system. *Engineering Structures.* **18:4**, 301–310.

Tsai, C.S. (1997). Finite element formulations for friction pendulum seismic isolation bearings. *International Journal for Numerical Methods In Engineering*. **40:1**, 29-49.

Zayas, V., Low, S., and Mahin, S. (1987). The FPS earthquake resisting system. Report No. CB/EERC-87/01, Earthquake Engineering Research Center, University of California, Berkeley, California.

Zayas, V., Low, S., Bozzo L., and Mahin, S. (1989). Feasibility and performance studies on improving the earthquakes resistance of new and existing buildings using the frictional pendulum system. Report No. CB/EERC-89/09, Earthquake Engineering Research Center, University of California, Berkeley, California.

Zayas, V., Low, S. and Mahin, S. (1990). A simple pendulum technique for achieving seismic isolation. *Earthquake Spectra.* **6:2**, 317-334.